Construction of an error map of rotary axes on a five-axis machining center by static R-test

Soichi Ibaraki[1] * , Chiaki Oyama[1] and Hisashi Otsubo[2]

[1] *Department of Micro Engineering, Kyoto University,*
Yoshida-honmachi, Sakyo-ku, Kyoto 606-8501, Japan.
[2] *Otsubo Engineering Research Center,*
Yuno 266-1, Kannabe-cho, Fukuyama, Hiroshima, 720-2121, Japan.

Abstract

This paper proposes an efficient and automated scheme to calibrate error motions of rotary axes on a five-axis machining center by using the R-test. During a five-axis measurement cycle, the R-test probing system measures the three-dimensional displacement of a sphere attached to the spindle in relative to the machine table. Location errors, defined in ISO 230-7, of rotary axes are the most fundamental error factors in the five-axis kinematics. A larger class of error motions can be modeled as geometric errors that vary depending on the angular position of a rotary axis. The objective of this paper is to present an algorithm to identify not only location errors, but also such position-dependent geometric errors, or "error map," of rotary axes. Its experimental demonstration is presented.

Key words: R-test, five-axis machine tool, calibration, error motion, location error, error map.

---

* Corresponding author. Phone/Fax: +81-75-753-5227
  Email address: `ibaraki@prec.kyoto-u.ac.jp` (Soichi Ibaraki[1]).

1 Introduction

Machine tools with two rotary axes to tilt and rotate a tool and/or a workpiece, in addition to three orthogonal linear axes, are collectively called five-axis machine tools. With an increasing need for machined components with geometric complexity in a high efficiency, they are extensively used in various manufacturing applications requiring higher machining accuracy. The improvement of their motion accuracies is a crucial demand in the market.

As a basis to improve the motion accuracy of five-axis machines, it is important to develop a methodology to measure it in an accurate, and efficient manner. ISO 10791-1∼3 [1] standards describe no-load or quasi-static measurements with the main focus on evaluating static position and orientation errors of the axis average line of a rotary axis. Such errors are called location errors in ISO 230-7 [2], or geometric errors [3], link errors [4] in the literature. The importance of location errors is well understood by many machine tool manufactures, as one of the most fundamental error factors in the five-axis kinematics. There has been many research works reported in the literature on the identification of location errors based on the measurement of the machine's positioning error. Typical ones include the application of the telescoping double ball bar (DBB) [3,5,6,7,8]. Its inclusion in the revision of ISO 10791-6 is currently under the discussion in ISO TC39/SC2 [9,10].

Although the ball bar measurement is widely accepted by machine tool builders world-wide, it has potentially critical issues in its application to five-axis machines. Since one setup of ball bar measurement only measures the displacement in one direction, it requires at least a couple of different setups to identify all location errors. It requires an experienced operator to be always with the measurement, and its full automation is difficult.

Weikert [11], Bringmann and Knapp [12] presented the "R-Test," where the three-dimensional displacement of a sphere attached to the spindle is mea-

sured by three (or four in [11,12]) linear displacement sensors installed on the table. Zargarbashi and Mayer [4] recently presented an analogous measurement instrument named CapBall with non-contact capacitive sensors. While the ball bar measurement is one-dimensional, the R-test collects a three-dimensional error trajectory in an automated measurement cycle, requiring no setup change. ISO TC39/SC2 has been discussing the inclusion of R-test, as well as ball bar measurements, in the revision of ISO 10791-6 [9,10]. Lately, IBS Precision Engineering [13,14] and Fidia [15] commercialized an R-test device for machine tool calibration.

In today's commercial CNC for machine tools, it is common to compensate a linear positioning error or a straightness error of a linear axis based on the pre-measured error map [16]. Analogous compensation of error motions of a rotary axis is possible. Compensation of location errors of a rotary axis has been demonstrated in the literature [17,18,19], and it can be easily extended to more complex errors. To implement such a compensation on mass-produced machines, the efficiency and the automation of error calibration are crucial. Compared to the ball bar, the R-test has a strong potential advantage in this aspect.

Bringmann and Knapp [12] presented the application of R-test to the identification of location errors of rotary axes. Zargarbashi and Mayer [4] also considers location errors only. On the latest small-sized five-axis machining centers, from our experiences, it is often the case that location errors are tuned sufficiently small in the machine assembly. In such a case, more complex error motions, such as the gravity deformation, angular positioning error of a rotary axis, "run-out" or "coning" of a rotary axis, can be dominant in the machining accuracy. This paper parameterizes such a larger class of error motions by geometric errors that vary depending on the angular position of a rotary axis. They are referred to as position-dependent geometric errors [20], which can be

3

seen as an "error map" of a rotary axis [16]. The objective of this paper is to propose the application of R-test to the identification of position-dependent geometric errors associated with each rotary axes. It will be experimentally demonstrated on a commercial five-axis machining center.

2   Error parameters to be identified in five-axis kinematic model

2.1   Machine configuration

This paper considers the 5-axis machine configuration with a titling rotary table depicted in Fig. 1. The machine has three linear-axis drives (X, Y, Z) and two rotary-axis drives (B,C). It must be emphasized that the basic idea of this paper can be straightforwardly extended to any configurations of five-axis machines.

2.2   Position-independent and position-dependent geometric errors

Location errors [2] define the position and the orientation of the axis average line of a rotary axis. ISO 230-7 [2] defines the axis average line as "a straight line segment located with respect to the reference coordinate axes representing the mean location of the axis of rotation." For the machine configuration depicted in Fig. 1, total eight location errors, shown in Table 1, are sufficient [21,3]. It is to be noted that many 5-axis kinematic models in the literature, including the one in ISO 230-7 [2,16], define each geometric error *in an absolute sense* with respect to the single machine (reference) coordinate system. In our model [21,6,17,22] geometric errors of each axis are defined *in a relative sense* with respect to the axis on which it is mounted. For example, geometric errors of C-axis are defined with respect to the position and the orientation of A-axis. Table 1 also shows the correspondence of our notation of error parameters with that in ISO 230-7 [2].

4

It is to be emphasized that location errors only represent *mean* location and orientation of axis of rotation. The location and the orientation may vary due to its rotation (described by the term "axis of rotation error motion" in ISO 230-7 [2]). A larger class of error motions can be modeled as geometric errors that vary depending on the angular position of a rotary axis [22]. They are referred to as position-dependent geometric errors [20] in this paper.

For example, location errors, δx_{BY}^0 and δz_{BY}^0, represent an offset of B-axis average line in X- and Z-directions. By parameterizing them dependent on B-axis angular position, denoted by $\delta x_{BY}(B)$ and $\delta y_{BY}(B)$, they can model a periodic pure radial error motion [2], or "run-out," of B-axis. Analogously, a periodic tilt error motion [2] of B-axis, often called "angular motion" [22] or "coning" [2] in the industry, can be modeled by $\alpha_{BY}(B)$ and $\gamma_{BY}(B)$. When the table is displaced in the Z-direction due to the gravity-induced deformation, it may be modeled by $\delta z_{BY}(B)$.

Table 2 shows position-dependent geometric errors for the machine configuration in Fig. 1. It is to be noted that parameters associated with B-axis are dependent only on the angular position of B-axis, while those associated with C-axis are dependent on both B- and C-axis angular positions. This is because an error motion of C-axis may be affected by B-axis angular position (its typical causes include gravity-induced deformation of bearings or mechanical structure).

In this paper, we represent position-dependent geometric errors as follows:

$$\delta x_{BY}(B) = \delta x_{BY}^0 + \delta \tilde{x}_{BY}(B) \tag{1}$$

where δx_{BY}^0 is constant. The symbol ˜ represents a position-dependent term. All parameters associated with B-axis, i.e. $\delta x_{BY}(B)$, $\delta y_{BY}(B)$, $\delta z_{BY}(B)$, $\alpha_{BY}(B)$, $\beta_{BY}(B)$, and $\gamma_{BY}(B)$, and two parameters associated with C-axis, namely $\delta x_{CB}(B,C)$ and $\alpha_{CB}(B,C)$, are represented analogously as a sum of constant

and position-dependent terms. Other C-axis parameters do not have a constant term; for example,

$$\delta y_{CB}(B_i, C_j) = \delta \tilde{y}_{CB}(B_i, C_j) \tag{2}$$

It is also important to note that this paper assumes geometric errors of linear axes (X, Y, and Z-axes) are negligibly small compared to those of rotary axes. As was reviewed in Section 1, many methodologies for 5-axis error calibration have been recently studied in the literature, such as 1) the ball bar test, 2) the R-test, 3) the test with a touch-trigger probe [23], 4) the test with a linear displacement sensor and an artifact (e.g. straightedge) [1], and 5) the test with a linear displacement sensor and a precision sphere [10]. Notice that all of them only measure the relative displacement of the spindle tip to the table, and it is therefore not possible to separate error motions of rotary axes and linear axes. Some of these works, e.g. [12], includes the identification of squareness errors or linear "expansion" of linear axes. They are just one of the most fundamental error motions of linear axes, and linear axes have to be assumed to have no more complex error motions.

To identify error motions of rotary axes, static error motions of linear axes are required to be separately pre-calibrated by conventional measurement (e.g. as shown in ISO 10791-1 [1]). If volumetric errors of linear axes are not sufficiently small compared to the influence of rotary axes, they must be properly compensated as in [16]. The influence of linear axis error motions to R-test measurements was discussed by Bringmann and Knapp [24].

2.3 Kinematic modeling of five-axis machine

The kinematic model to compute the tool center position in relative to the workpiece is the basis of the error calibration presented in this paper. Although its derivation can be found in many previous publications [3,21,25,26], this subsection only briefly reviews it.

6

Define the reference coordinate system (X-Y-Z) as the coordinate system fixed to the machine frame or bed. Suppose that X^*, Y^*, Z^*, B^* and $C^* \in \mathbb{R}$ represent the command position of X, Y, Z, B, and C axes, respectively. Since linear axes are assumed to have no geometric error, the tool center location in the reference frame is given by $^r q := [\, X^* \ Y^* \ Z^* \,]^T$. The left-side superscript r represents a vector in the reference coordinate system. The superscript $*$ represents reference (commanded) values or vectors.

Define the workpiece coordinate system (^wX-^wY-^wZ) as the coordinate system attached to the rotary table. The homogeneous transformation matrix (HTM) representing the transformation from the workpiece coordinate system to the reference coordinate system is given by:

$$
\begin{aligned}
^r T_w &= {}^y T_b {}^b T_c \\
^b T_c &= D_x(\delta x_{CB}(B^*, C^*) D_y(\delta y_{CB}(B^*, C^*)) D_z(\delta z_{CB}(B^*, C^*)) \\
&\qquad D_a(\alpha_{CB}(B^*, C^*)) D_b(\beta_{CB}(B^*, C^*)) D_c(\gamma_{CB}(B^*, C^*)) D^c(-C^*) \\
^y T_b &= D_x(\delta x_{BY}(B^*)) D_y(\delta y_{BY}(B^*)) D_z(\delta z_{BY}(B^*)) \\
&\qquad D_a(\alpha_{BY}(B^*)) D_b(\beta_{BY}(B^*)) D_c(\gamma_{BY}(B^*)) D^b(-B^*)
\end{aligned}
\tag{3}
$$

where $D_x(x)$, $D_y(y)$, and $D_z(z)$ represent the HTM for linear motions in X-, Y-, and Z-directions. $D_a(a)$, $D_b(b)$, and $D_c(c)$ represent the HTM for angular motions about X, Y and Z axes. They are respectively given by (e.g. [25,26]):

$$
D_x(x) = \begin{bmatrix} 1 & 0 & 0 & x \\ 0 & 1 & 0 & 0 \\ 0 & 0 & 1 & 0 \\ 0 & 0 & 0 & 1 \end{bmatrix}, \quad D_y(y) = \begin{bmatrix} 1 & 0 & 0 & 0 \\ 0 & 1 & 0 & y \\ 0 & 0 & 1 & 0 \\ 0 & 0 & 0 & 1 \end{bmatrix}
$$

$$
D_z(z) = \begin{bmatrix} 1 & 0 & 0 & 0 \\ 0 & 1 & 0 & 0 \\ 0 & 0 & 1 & z \\ 0 & 0 & 0 & 1 \end{bmatrix}, \quad D_a(a) = \begin{bmatrix} 1 & 0 & 0 & 0 \\ 0 & \cos a & -\sin a & 0 \\ 0 & \sin a & \cos a & 0 \\ 0 & 0 & 0 & 1 \end{bmatrix}
\tag{4}
$$

$$
D_b(b) = \begin{bmatrix} \cos b & 0 & \sin b & 0 \\ 0 & 1 & 0 & 0 \\ -\sin b & 0 & \cos b & 0 \\ 0 & 0 & 0 & 1 \end{bmatrix}, \quad D_c(c) = \begin{bmatrix} \cos c & -\sin c & 0 & 0 \\ \sin c & \cos c & 0 & 0 \\ 0 & 0 & 1 & 0 \\ 0 & 0 & 0 & 1 \end{bmatrix}
$$

Hence, the tool center location in the workpiece coordinate system, $^{w}q \in \mathbb{R}^3$, is given by:

$$\begin{bmatrix} ^{w}q \\ 1 \end{bmatrix} = (^{r}T_w)^{-1} \cdot \begin{bmatrix} ^{r}q \\ 1 \end{bmatrix} \tag{5}$$

The left-side superscript w denotes the vector defined in the workpiece coordinate system.

3   Measurement device and procedure

Figure 2 depicts the R-test device used in this study. A ceramic precision sphere is attached to the machine spindle. Three contact-type linear displacement probes are installed on the rotary table. Since the probing system is fixed on the table, it measures the sphere displacement *in the workpiece coordinate system*. Major specifications of the linear displacement probe are shown in Table 3. The probes are calibrated over the entire measuring range by the probe's manufacturer.

The following parameters must be calibrated in advance: 1) unit vectors representing sensor directions. and 2) the center shift of sphere from the spindle axis average line. Their calibration procedure was presented in previous studies [27].

In a measurement cycle, the machine table is indexed at B- and C-angular positions, B_i^* $(i = 1,\cdots,N_b)$ and C_j^* $(j = 1,\cdots,N_c)$. Measurement poses, B_i^* and C_j^*, must be distributed over the entire workspace of each rotary axis. The X, Y, and Z axes are positioned such that the sphere follows the R-test probing system. The nominal sphere position in the global coordinate system, denoted by $^{r}q^*(B_i^*,C_j^*) \in \mathbb{R}^3$, is given by:

$$\begin{bmatrix} ^{r}q^*(B_i^*,C_j^*) \\ 1 \end{bmatrix} = D_b(-B_i^*)D_c(-C_j^*) \begin{bmatrix} ^{w}q^* \\ 1 \end{bmatrix} \tag{6}$$

where $^w q^* = \begin{bmatrix} ^w q_x^*, ^w q_y^*, ^w q_z^* \end{bmatrix} \in \mathbb{R}^3$ is a constant vector representing the nominal sphere position in the workpiece coordinate system.

4 Identification of location errors

This section first presents a formulation to identify location errors shown in Table 1 from a set of sphere displacements measured by R-test. Although the identification of location errors has been already presented by Bringmann and Knapp [12], we start from its brief review as the basis. The final objective of this paper is to extend this formulation to identify position-dependent geometric errors shown in Table 2. It is to be noted that Bringmann and Knapp [12] only presented numerically-computed Jacobian matrix of the five-axis kinematics; we will present its analytical formulation.

4.1 Jacobian matrix

Denote a set of location errors to be identified shown in Table 1 by:

$$\omega_0 := [\delta x_{BY}^0, \delta y_{BY}^0, \delta z_{BY}^0, \alpha_{BY}^0, \beta_{BY}^0, \gamma_{BY}^0, \delta x_{CB}^0, \alpha_{CB}^0]^T \tag{7}$$

For the reference poses B_i^* $(i = 1, \cdots, N_b)$ and C_j^* $(j = 1, \cdots, N_c)$, suppose that the actual sphere position in the workpiece coordinate system is measured by the R-test as $^w q(B_i^*, C_j^*) = \begin{bmatrix} ^w q_x(B_i^*, C_j^*), ^w q_y(B_i^*, C_j^*), ^w q_z(B_i^*, C_j^*) \end{bmatrix}^T$. Denote the Jacobian matrix of the function relating w_0 to $^w q(B_i^*, C_j^*)$ by:

$$\frac{\partial^w q(B_i^*, C_j^*)}{\partial \omega_0} := \begin{bmatrix} \frac{\partial^w q_x(B_i^*, C_j^*)}{\partial \omega_0(1)} & \cdots & \frac{\partial^w q_x(B_i^*, C_j^*)}{\partial \omega_0(8)} \\ \frac{\partial^w q_y(B_i^*, C_j^*)}{\partial \omega_0(1)} & \cdots & \frac{\partial^w q_y(B_i^*, C_j^*)}{\partial \omega_0(8)} \\ \frac{\partial^w q_z(B_i^*, C_j^*)}{\partial \omega_0(1)} & \cdots & \frac{\partial^w q_z(B_i^*, C_j^*)}{\partial \omega_0(8)} \end{bmatrix} \tag{8}$$

From Eqs. (3)(5) and (6), we have:

9

$$\begin{bmatrix} {}^{w}q(B_i^*, C_j^*) \\ 1 \end{bmatrix} = \left({}^{r}T_w\right)^{-1} \cdot \begin{bmatrix} {}^{r}q^*(B_i^*, C_j^*) \\ 1 \end{bmatrix}$$

$$= \left\{ D_x(\delta x_{BY}^0) \ldots D_c(\gamma_{BY}^0) D_b(-B_i^*) D_x(\delta x_{CB}^0) D_a(\alpha_{CB}^0) D_c(-C_j^*) \right\}^{-1} \cdot$$

$$D_b(-B_i^*) D_c(-C_j^*) \begin{bmatrix} {}^{w}q^* \\ 1 \end{bmatrix}$$

$$= D_c(C_j^*) D_a(-\alpha_{CB}^0) D_x(-\delta x_{CB}^0) \cdot$$

$$\{ D_b(B_i^*) D_c(-\gamma_{BY}^0) \ldots D_x(-\delta x_{BY}^0) D_b(-B_i^*) \} D_c(-C_j^*) \begin{bmatrix} {}^{w}q^* \\ 1 \end{bmatrix} \tag{9}$$

In this paper, we assume that all the (position-independent or position-dependent) geometric parameters to be identified are sufficiently small. Note that, when ΔA ΔB and ΔC are sufficiently small, the following approximation generally holds:

$$D_a(\Delta A) D_b(\Delta B) D_c(\Delta C) \approx \begin{bmatrix} 1 & -\Delta C & \Delta B & 0 \\ \Delta C & 1 & -\Delta A & 0 \\ -\Delta B & \Delta A & 1 & 0 \\ 0 & 0 & 0 & 1 \end{bmatrix} \tag{10}$$

By using it, when $\Delta X, \cdots, \Delta C$ are sufficiently small, we have:

$$\begin{aligned} D_b(B_i^*) D_x(\Delta X) D_b(-B_i^*) &\approx D_x(\Delta X \cos B_i^*) D_z(-\Delta X \sin B_i^*) \\ D_b(B_i^*) D_y(\Delta Y) D_b(-B_i^*) &\approx D_y(\Delta Y) \\ D_b(B_i^*) D_z(\Delta Z) D_b(-B_i^*) &\approx D_x(\Delta Z \sin B_i^*) D_z(\Delta Z \cos B_i^*) \\ D_b(B_i^*) D_a(\Delta A) D_b(-B_i^*) &\approx D_a(\Delta A \cos B_i^*) D_c(-\Delta A \sin B_i^*) \\ D_b(B_i^*) D_b(\Delta B) D_b(-B_i^*) &\approx D_b(\Delta B) \\ D_b(B_i^*) D_c(\Delta C) D_b(-B_i^*) &\approx D_a(\Delta C \sin B_i^*) D_c(\Delta C \cos B_i^*) \end{aligned} \tag{11}$$

Analogous approximations can be derived for $D_c(C_j^*) D_*(*) D_c(-C_j^*)$. By using these approximations, Eq. (9) can be rewritten by:

$$\begin{bmatrix} {}^{w}q(B_i^*, C_j^*) \\ 1 \end{bmatrix} \approx D_x(\Delta X) D_y(\Delta Y) D_z(\Delta Z) D_a(\Delta A) D_b(\Delta B) D_c(\Delta C) \begin{bmatrix} {}^{w}q^* \\ 1 \end{bmatrix} \tag{12}$$

where

$$\Delta X = -(\delta x_{BY}^0 \cos B_i^* + \delta z_{BY}^0 \sin B_i^* + \delta x_{CB}^0) \cos C_j^* + \delta y_{BY}^0 \sin C_j^*$$
$$\Delta Y = -(\delta x_{BY}^0 \cos B_i^* + \delta z_{BY}^0 \sin B_i^* + \delta x_{CB}^0) \sin C_j^* - \delta y_{BY}^0 \cos C_j^*$$
$$\Delta Z = \delta x_{BY}^0 \sin B_i^* - \delta z_{BY}^0 \cos B_i^* \tag{13}$$
$$\Delta A = -(\alpha_{BY}^0 \cos B_i^* + \gamma_{BY}^0 \sin B_i^* + \alpha_{CB}^0) \cos C_j^* + \beta_{BY}^0 \sin C_j^*$$
$$\Delta B = -(\alpha_{BY}^0 \cos B_i^* + \gamma_{BY}^0 \sin B_i^* + \alpha_{CB}^0) \sin C_j^* - \beta_{BY}^0 \cos C_j^*$$
$$\Delta C = \alpha_{BY}^0 \sin B_i^* - \gamma_{BY}^0 \cos B_i^*$$

The formulation (12), with the approximation (10), represents the sphere displacement $^w q(B_i^*, C_j^*)$ as a linear function of each parameter in ω_0. It gives, therefore, a unique solution for ω_0. The Jacobian matrix (8) can be derived by partially differentiating Eq. (12) by each parameter in ω_0. For example, its partial derivative with respect to β_{BY}^0 is:

$$\frac{\partial^w q(B_i^*, C_j^*)}{\partial \beta_{BY}^0} = \begin{bmatrix} -\cos C_j^* \cdot {}^w q_z^* \\ -\sin C_j^* \cdot {}^w q_z^* \\ \cos C_j^* \cdot {}^w q_x^* + \sin C_j^* \cdot {}^w q_y^* \end{bmatrix} \tag{14}$$

4.2   Identification of location errors

It is important to note that R-test probes can only measure the displacement of sphere center from its initial position. For the simplicity of notation, $B_i^* = C_j^* = 0°$ $(i = j = 1)$ is called the initial position in this paper. For the reference poses B_i^* $(i = 1, \cdots, N_b)$ and C_j^* $(j = 1, \cdots, N_c)$, the sphere displacement measured by R-test probes is represented by:

$$^w \bar{q}(B_i^*, C_j^*) = {}^w q(B_i^*, C_j^*) - {}^w q(B_1^*, C_1^*) \tag{15}$$

The symbol ‾ represents the measured displacement. The restriction, $^w \bar{q}(B_1^*, C_1^*) = \begin{bmatrix} 0 & 0 & 0 \end{bmatrix}^T$, is called "initial resetting" hereafter.

Then, a set of location errors (7), $\hat{\omega}_0$, is identified by solving the following problem by using the least square method:

$$\min_{\hat{\omega}_0} \sum_{i,j} \left\| {}^w \bar{q}(B_i^*, C_j^*) - \left(\frac{\partial^w q(B_i^*, C_j^*)}{\partial \omega_0} - \frac{\partial^w q(B_1^*, C_1^*)}{\partial \omega_0} \right) \hat{\omega}_0 \right\|^2 \tag{16}$$

where $\| * \|$ represents the 2-norm.

11

5   Identification of position-dependent geometric errors

5.1   Measurement Procedure

The sphere displacement measured by the R-test is influenced by both B- and C-axis error motions. The objective of the algorithm presented in this section is to separate the influence of B- and C-axis error motions from R-test results, and to construct an error map, or position-dependent geometric errors, for each of B- and C-axes separately.

It is clearly not possible to observe C-axis tilt error motions from measuring the displacement of single sphere only. To observe it, the R-test measurement cycle must be repeated with three different sphere positions. Figure 3 illustrates three nominal sphere locations in the workpiece coordinate system, ${}^{w}q_i^*$ $(i = 1, 2, 3)$.

5.2   Redundancy due to initial resetting

As was discussed in Section 4.2, since linear displacement sensors used in our R-test device is incremental, all sensor outputs are restricted to be zero at the initial position (i.e. $B_i^* = C_j^* = 0°$ $(i = j = 1)$). Therefore, the influence of geometric errors on this initial position are included in all the R-test measurements, ${}^{w}q(B_i^*, C_j^*)$, as shown in Eq. (15).

As an illustrative example, suppose that $\delta z_{BY}(B_i^*) = \delta z_{BY}^0$ and all other parameters are zero. Then, from Eqs. (12)(13) and (15), we have:

$$
{}^{w}\bar{q}(B_i^*, C_1^*) = \begin{bmatrix} -\delta z_{BY}^0 \sin B_i^* \\ 0 \\ -\delta z_{BY}^0 \cos B_i^* + \delta z_{BY}^0 \end{bmatrix} \tag{17}
$$

where $C_j^* = 0°$ $(j = 1)$. It can be easily seen that the following position-dependent errors result in exactly the same sphere displacement in Eq. (17):

$$\delta x_{BY}(B_i^*) = \delta x_{BY}^0 \cos B_i^*$$
$$\delta z_{BY}(B_i^*) = \delta z_{BY}^0 + \delta x_{BY}^0 \sin B_i^* \tag{18}$$

with an arbitrary constant δx_{BY}^0. These two cases cannot be distinguished from measured sphere displacements (17). Notice that this redundancy is caused by the initial resetting. In practice, however, the constant error, $\delta z_{BY}(B_i^*) = \delta z_{BY}^0$, is more likely, typically caused by the miscalibration of the position of B-axis of rotation (or, equivalently, the miscalibration of the tool length). Therefore, in many applications, it is reasonable to first identify constant terms, δz_{BY}^0 in this example, and then to model the residual as position-dependent terms.

5.3 Identification of position-independent terms

In practice, the miscalibration of the position of rotation center of a rotary axis, or the miscalibration of the tool length, are often among the most critical error factors in the 5-axis kinematics. In this paper, they are modeled as position-independent terms; for example, the miscalibration of the rotation center of B-axis average line is represented by δx_{BY}^0 and δz_{BY}^0, and the miscalibration of the tool length is included in δz_{BY}^0. This section first presents the identification of these position-independent terms. The primal interest of this paper is in the identification of more complex error motions of each rotary axis modeled as position-dependent geometric errors, which will be presented in Section 5.4.

As described in Eq. (1), geometric errors are represented as a sum of position-independent and position-dependent terms. Total eight position-independent terms, namely:

$$\hat{\omega}_0 := \left[\delta x_{BY}^0, \delta y_{BY}^0, \delta z_{BY}^0, \alpha_{BY}^0, \beta_{BY}^0, \gamma_{BY}^0, \delta x_{CB}^0, \alpha_{CB}^0 \right] \tag{19}$$

are first identified. Let:

$$\delta x^0_{BY} = \delta x_{BY}(B^*_1), \quad \delta y^0_{BY} = \delta y_{BY}(B^*_1)$$
$$\alpha^0_{BY} = \alpha_{BY}(B^*_1), \quad \beta^0_{BY} = \beta_{BY}(B^*_1) \tag{20}$$
$$\delta x^0_{CB} = \underset{j}{\text{mean}}\left\{\delta x_{CB}(B^*_1, C^*_j)\right\}, \quad \alpha^0_{CB} = \underset{j}{\text{mean}}\left\{\delta x_{CB}(B^*_1, C^*_j)\right\}$$

where $B^*_1 = 0°$. Then, $\hat{\omega}_{01} := [\delta x^0_{BY} + \delta x^0_{CB}, \delta y^0_{BY}, \alpha^0_{BY} + \alpha^0_{CB}, \beta^0_{BY}]$ can be identified by solving the following problem analogously as in Eq. (16):

$$\min_{\hat{\omega}_{01}} \sum_j \left\| {}^w\bar{q}(B^*_1, C^*_j) - \left(\frac{\partial^w q(B^*_1, C^*_j)}{\partial \omega_{01}} - \frac{\partial^w q(B^*_1, C^*_1)}{\partial \omega_{01}}\right)\hat{\omega}_{01}\right\|^2 \tag{21}$$

$\hat{\omega}_{01}$ is identified only by a set of sphere displacements measured at $B^*_1 = 0°$ such that B-axis error motions impose no influence. The other set of position-independent terms, $\hat{\omega}_{02} := [\delta x^0_{BY}, \delta z^0_{BY}, \alpha^0_{BY}, \gamma^0_{BY}]$, cannot be identified without moving the B-axis. It is identified by solving:

$$\min_{\hat{\omega}_{02}} \sum_i \left\| {}^w\bar{q}(B^*_i, C^*_1) - \left(\frac{\partial^w q(B^*_i, C^*_1)}{\partial \omega_{02}} - \frac{\partial^w q(B^*_1, C^*_1)}{\partial \omega_{02}}\right)\hat{\omega}_{02}\right\|^2 \tag{22}$$

5.4 Identification of position-dependent geometric errors associated with B-axis

By using position-dependent geometric errors shown in Table 2, the formulation (12) is extended to:

$${}^w q(B^*_i, C^*_j) = D_x(\Delta X)D_y(\Delta Y)D_z(\Delta Z)D_a(\Delta A)D_b(\Delta B)D_c(\Delta C){}^w q^*$$

$$\begin{aligned}
\Delta X = &-(\delta x_{BY}(B^*_i)\cos B^*_i + \delta z_{BY}(B^*_i)\sin B^*_i + \delta x_{CB}(B^*_i, C^*_j))\cos C^*_j \\
&+(\delta y_{BY}(B^*_i) + \delta y_{CB}(B^*_i, C^*_j))\sin C^*_j \\
\Delta Y = &-(\delta x_{BY}(B^*_i)\cos B^*_i + \delta z_{BY}(B^*_i)\sin B^*_i + \delta x_{CB}(B^*_i, C^*_j))\sin C^*_j \\
&-(\delta y_{BY}(B^*_i) + \delta y_{CB}(B^*_i, C^*_j))\cos C^*_j \\
\Delta Z = &\,\delta x_{BY}(B^*_i)\sin B^*_i - \delta z_{BY}(B^*_i)\cos B^*_i - \delta z_{CB}(B^*_i, C^*_j) \qquad (23)\\
\Delta A = &-(\alpha_{BY}(B^*_i)\cos B^*_i + \gamma_{BY}(B^*_i)\sin B^*_i + \alpha_{CB}(B^*_i, C^*_j))\cos C^*_j \\
&+(\beta_{BY}(B^*_i) + \beta_{CB}(B^*_i, C^*_j))\sin C^*_j \\
\Delta B = &-(\alpha_{BY}(B^*_i)\cos B^*_i + \gamma_{BY}(B^*_i)\sin B^*_i + \alpha_{CB}(B^*_i, C^*_j))\sin C^*_j \\
&-(\beta_{BY}(B^*_i) + \beta_{CB}(B^*_i, C^*_j))\cos C^*_j \\
\Delta C = &\,\alpha_{BY}(B^*_i)\sin B^*_i - \gamma_{BY}(B^*_i)\cos B^*_i - \gamma_{CB}(B^*_i, C^*_j)
\end{aligned}$$

14

The influence of position-independent terms, $\hat{\omega}_0$, on the measured sphere displacement, $^w\bar{q}(B_i^*, C_j^*)$, is represented by:

$$^w\hat{q}^0(B_i^*, C_j^*) \approx D_x(\Delta X)D_y(\Delta Y)D_z(\Delta Z)D_a(\Delta A)D_b(\Delta B)D_c(\Delta C)^w q^*$$
$$^w\hat{\bar{q}}^0(B_i^*, C_j^*) = {}^w\hat{q}^0(B_i^*, C_j^*) - {}^w\hat{q}^0(B_1^*, C_1^*) \tag{24}$$

where $\Delta X, \cdots, \Delta C$ are given in Eq. (13). The symbol ˆ represents the simulated position by using identified error parameters. Position-dependent terms are identified by subtracting $^w\hat{\bar{q}}^0(B_i^*, C_j^*)$ from measured sphere displacements, $^w\bar{q}(B_i^*, C_j^*)$.

First, to avoid the redundancy, position-dependent terms in C-axis error motions are assumed to meet:

$$\sum_j \left\{ \begin{bmatrix} \cos C_j^* & \sin C_j^* & 0 \\ -\sin C_j^* & \cos C_j^* & 0 \\ 0 & 0 & 1 \end{bmatrix} \begin{bmatrix} \delta\tilde{x}_{CB}(B_i^*, C_j^*) \\ \delta\tilde{y}_{CB}(B_i^*, C_j^*) \\ \delta\tilde{z}_{CB}(B_i^*, C_j^*) \end{bmatrix} \right\} = \begin{bmatrix} 0 \\ 0 \\ 0 \end{bmatrix}$$
$$\sum_j \left\{ \begin{bmatrix} \cos C_j^* & \sin C_j^* & 0 \\ -\sin C_j^* & \cos C_j^* & 0 \\ 0 & 0 & 1 \end{bmatrix} \begin{bmatrix} \tilde{\alpha}_{CB}(B_i^*, C_j^*) \\ \tilde{\beta}_{CB}(B_i^*, C_j^*) \\ \tilde{\gamma}_{CB}(B_i^*, C_j^*) \end{bmatrix} \right\} = \begin{bmatrix} 0 \\ 0 \\ 0 \end{bmatrix} \tag{25}$$

which suggests that, in the workpiece coordinate system, the mean of $\left[\delta\tilde{x}_{CB}(B_i^*, C_j^*), \delta\tilde{y}_{CB}(B_i^*, C_j^*), \delta\tilde{z}_{CB}(B_i^*, C_j^*) \right]$ $\left(\left[\tilde{\alpha}_{CB}(B_i^*, C_j^*), \tilde{\beta}_{CB}(B_i^*, C_j^*), \tilde{\gamma}_{CB}(B_i^*, C_j^*) \right] \right)$ $(j = i, \cdots, N_c)$ is at the origin.
Then, from the first equation in Eq. (23), we have:

$$\sum_j \Delta X = \sum_j \{ -(\delta x_{BY}(B_i^*) \cos B_i^* + \delta z_{BY}(B_i^*) \sin B_i^* + \delta x_{CB}^0) \cos C_j^*$$
$$+ (\delta y_{BY}(B_i^*) + \delta y_{CB}^0) \sin C_j^* \} \tag{26}$$

where position-dependent error motions of C-axis impose no influence. The same observation can be made on all equations in Eq. (23). Therefore, at each

B_i^* $(i = 1, \cdots, N_c)$,

$$\omega_B(B_i^*) := \left[\delta \tilde{x}_{BY}(B_i^*), \delta \tilde{y}_{BY}(B_i^*), \delta \tilde{z}_{BY}(B_i^*), \tilde{\alpha}_{BY}(B_i^*), \tilde{\beta}_{BY}(B_i^*), \tilde{\gamma}_{BY}(B_i^*) \right],$$
(27)

can be identified by solving:

$$\min_{\hat{\omega}_B(B_i^*)} \sum_j \left\| \left({}^w\bar{q}(B_i^*, C_j^*) - {}^w\hat{\bar{q}}^0(B_i^*, C_j^*) \right) - \left(\frac{\partial^w q(B_i^*, C_j^*)}{\partial \omega_B(B_i^*)} - \frac{\partial^w q(B_1^*, C_1^*)}{\partial \omega_B(B_i^*)} \right) \hat{\omega}_B(B_i^*) \right\|^2$$
(28)

where the Jacobian matrix, $\frac{\partial^w q(B_i^*, C_j^*)}{\partial \omega_B(B_i^*)}$, can be derived from Eq. (23).

5.5 *Identification of position-dependent geometric errors associated with C-axis*

First, define *the B-axis coordinate system* (${}^bX$-${}^bY$-${}^bZ$) as the coordinate system fixed on the B-axis. In this coordinate system, the measured sphere position is described by:

$$\begin{bmatrix} {}^b\bar{q}(B_i^*, C_j^*) \\ 1 \end{bmatrix} := D_c(-C_j^*) \begin{bmatrix} {}^w\bar{q}(B_i^*, C_j^*) \\ 1 \end{bmatrix}$$
(29)

where the left-hand side superscript ^{b} represents a vector in the B-axis coordinate system.

The influence of the identified $\hat{\omega}_0$ (Eq. (19)) and $\hat{\omega}_B(B_i^*)$ (Eq. (27)) on the measured sphere position, ${}^w\bar{q}(B_i^*, C_j^*)$, is given from Eq. (9) by:

$$\begin{aligned} \begin{bmatrix} {}^b\hat{q}(B_i^*, C_j^*) \\ 1 \end{bmatrix} &:= {}^b\hat{T}_w \begin{bmatrix} {}^wq^* \\ 1 \end{bmatrix} \\ {}^b\hat{T}_w &:= D_a(-\alpha_{CB}^0) D_x(-\delta x_{CB}^0) D_b(B_i^*) D_c(-\gamma_{BY}(B_i^*)) \ldots \\ &\quad D_x(-\delta x_{BY}(B_i^*)) D_b(-B_i^*) D_c(-C_j^*) \\ {}^b\hat{\bar{q}}(B_i^*, C_j^*) &:= {}^b\hat{q}(B_i^*, C_j^*) - {}^b\hat{q}(B_1^*, C_1^*) \end{aligned}$$
(30)

Then, define:

$$ {}^b\bar{p}(B_i^*, C_j^*) := {}^b\bar{q}(B_i^*, C_j^*) - {}^b\hat{\bar{q}}(B_i^*, C_j^*) $$
(31)

16

which represents the influence of C-axis error motions only.

As has been stated in Section 5.1, tilt and angular error motions of C-axis are identified by observing two sets of measured sphere displacements at different locations. The tilt error motion of C-axis around the ^{b}X-axis, $\tilde{\alpha}_{CB}(B_i^*, C_j^*)$, is computed by comparing ${}^{b}\bar{p}(B_i^*, C_j^*)$ at #1 and #2 in Fig. 3:

$$\tilde{\alpha}_{CB}(B_i^*, C_j^*) = -\text{angle}_{YZ}\left\{{}^{b}\bar{p}_2(B_i^*, C_j^*) - {}^{b}\bar{p}_1(B_i^*, C_j^*), {}^{b}q_2^*(C_j^*) - {}^{b}q_1^*(C_j^*)\right\}$$
(32)

where ${}^{b}q_n^*(C_j^*)$ ($n = 1, 2$) represents the nominal sphere position for #1 and #2 in the B-axis coordinate system. The function $\text{angle}_{YZ}(a, b)$ represents the angle of the projection of a vector $a \in \mathbb{R}^3$ to the YZ plane with respect to that of $b \in \mathbb{R}^3$. When $a = [a_x, a_y, a_z]^T$ and $b = [b_x, b_y, b_z]^T$, it is given by:

$$\text{angle}_{YZ}\left\{a, b\right\} := \cos^{-1}\frac{a_x b_x + a_z b_z}{\sqrt{a_x^2 + a_z^2}\sqrt{b_x^2 + b_z^2}}$$
(33)

Analogously, we have:

$$\tilde{\beta}_{CB}(B_i^*, C_j^*) = -\text{angle}_{XZ}\left\{{}^{b}\bar{p}_2(B_i^*, C_j^*) - {}^{b}\bar{p}_1(B_i^*, C_j^*), {}^{b}q_2^*(C_j^*) - {}^{b}q_1^*(C_j^*)\right\}$$
$$\tilde{\gamma}_{CB}(B_i^*, C_j^*) = -\text{angle}_{XY}\left\{{}^{b}\bar{p}_3(B_i^*, C_j^*) - {}^{b}\bar{p}_1(B_i^*, C_j^*), {}^{b}q_3^*(C_j^*) - {}^{b}q_1^*(C_j^*)\right\}$$
(34)

Finally, translational error motions of C-axis, namely $\delta\tilde{x}_{CB}(B_i^*, C_j^*)$, $\delta\tilde{y}_{CB}(B_i^*, C_j^*)$, and $\delta\tilde{z}_{CB}(B_i^*, C_j^*)$ ($i = 1, \cdots, N_b$, $j = 1, \cdots, N_c$), are identified to meet Eq. (23). They can be computed by eliminating the influence of identified $\tilde{\alpha}_{CB}(B_i^*, C_j^*)$, $\tilde{\beta}_{CB}(B_i^*, C_j^*)$ and $\tilde{\gamma}_{CB}(B_i^*, C_j^*)$ from ${}^{b}\bar{p}_1(B_i^*, C_j^*)$:

$$\begin{bmatrix} \delta\tilde{x}_{CB}(B_i^*, C_j^*) \\ \delta\tilde{y}_{CB}(B_i^*, C_j^*) \\ \delta\tilde{z}_{CB}(B_i^*, C_j^*) \\ 1 \end{bmatrix} = \begin{bmatrix} {}^{b}\bar{p}_1(B_i^*, C_j^*) \\ 1 \end{bmatrix}$$

$$-D_a(\tilde{\alpha}_{CB}(B_i^*, C_j^*))D_b(\tilde{\beta}_{CB}(B_i^*, C_j^*))D_c(\tilde{\gamma}_{CB}(B_i^*, C_j^*))\begin{bmatrix} {}^{w}q_1^* \\ 1 \end{bmatrix}$$
(35)

6 Experimental demonstration

6.1 Experimental setup

To illustrate the present error map construction scheme, its experimental application to a commercial small-sized 5-axis machining center will be presented. Its configuration is shown in Fig. 1, and its major specifications are shown in Table 4.

Its C-axis (rotary table) has a well-calibrated rotary encoder to the axis of rotation, and we thus assume that the C-axis angular positioning error is sufficiently small. Thus, to simplify the measurement procedure, only Measurements #1 and #2 in Fig. 3 are performed. The nominal sphere locations in the workpiece coordinate system are:

$$
\begin{aligned}
{}^{w}p_1^* &= [-42.30, -2.00, 147.72] \quad \text{(mm)} \\
{}^{w}p_2^* &= [-42.77, -0.60, 307.42] \quad \text{(mm)}
\end{aligned}
\tag{36}
$$

In this experiment, command B and C angular positions are given by:

$$
\begin{aligned}
B_i^* &= -90°, -60°, \cdots, 90° \quad (i = 1, \cdots, 7) \\
C_j^* &= 0°, 30°, \cdots, 330° \quad (j = 1, \cdots, 12)
\end{aligned}
\tag{37}
$$

Total $7 \times 12 = 84$ points are measured. Figure 4 shows command X^*, Y^*, Z^*, B^*, and C^* trajectories for Measurements #1 and #2.

Prior to experiments, the volumetric accuracy of linear axes (X, Y, and Z axes) of the experimental machining center was evaluated. By the machine manufacturer's standard calibration procedure based on ISO 10791-2, linear positioning errors, straightness errors, and squareness errors of linear axes were pre-calibrated. By combining them, the combined standard uncertainty of three-dimensional positioning by linear axes within their moving range (X298×Y85×Z191 mm in Measurement #1, and X615×Y85×Z350 mm in Measurement #2) is estimated 4.9 μm in Measurement #1, and 8.7 μm in

18

Measurement #2.

6.2   Measurement result

Figure 5 shows sphere displacements measured by R-test probes, ${}^w\bar{q}(B_i^*, C_j^*)$, in the workpiece coordinate system. For more intuitive understanding, they are viewed in the global coordinate system by:

$$ {}^r\bar{q}(B_i^*, C_j^*) = D_b(-B_i^*)D_c(-C_j^*)\,{}^w\bar{q}(B_i^*, C_j^*) \tag{38} $$

Figures 6(a) and (b) show measured $-{}^r\bar{q}(B_i^*, C_j^*)$ at $B_i^* = -90°$ and $B_i^* = 0°$ as examples. Note that $-{}^r\bar{q}(B_i^*, C_j^*)$ represents the position error of the R-test probe system in relative to the sphere attached to the spindle. Assuming that linear axes have no positioning error, it represents the table displacement. It is hereby referred to as measured probe displacements.

In Fig. 6, the error from the reference position is magnified by 10,000 times. "Table" represents rough location of rotary table. Fig. 6 only shows the projection of measured three-dimensional displacements onto the XZ plane. As another example, Fig. 7 shows their projection onto the XY plane of the B-axis coordinate system (i.e. the top view from the table) at $B_i^* = -90°$ and $0°$.

Many observations can be made on these plots to intuitively understand the machine's error motions. For example:

- At $B_i^* = -90°$ (Fig. 6(a)), measured trajectories is shifted from reference positions to +X direction by about 20 μm, and to -Z direction by about 25 μm. The largest contributor for this error is the mis-calibration of B-axis center position, parameterized by δx_{BY}^0 and δz_{BY}^0.

- At all B_i^*'s, the diameter of measured trajectories is enlarged by about 15 μm. This is mostly caused by the mis-calibration of C-axis center position,

parameterized by δy_{BY}^0 and $\delta x_{BY}^0 + \delta x_{CB}^0$.

- At $B_i^* = -90°$ (Fig. 6(a)), measured trajectories are slightly tilted from the vertical direction. This represents a small B-axis angular positioning error.

- At $B_i^* = -90°$ (Fig. 6(a)), no significant difference is observed in diameters of measured trajectories in Measurements #1 and #2. This suggests that no significant tilt error motion (or "coning") of C-axis is observed.

6.3   Construction of error map

(1)   Identification of position-independent terms

First, by using the algorithm presented in Section 5.3, total eight position-independent terms (19) are identified. Table 5 shows identified values.

The contribution of position-independent terms in measured probe displacements is studied by Eq. (24). Figure 8 compares measured displacements at $B_i^* = -90°$ (same as in Fig. 6(a)) and the simulated influence of parameters in Table 5. Such a comparison shows that position-independent terms, $\hat{\omega}_0$, are, in this particular case, largest contributors for measured displacements.

(2)   Identification of position-dependent geometric errors of B-axis

Position-dependent geometric errors of B-axis, namely $\delta x_{BY}(B_i^*)$, $\delta y_{BY}(B_i^*)$, $\delta z_{BY}(B_i^*)$, $\alpha_{BY}(B_i^*)$, $\beta_{BY}(B_i^*)$, and $\gamma_{BY}(B_i^*)$ ($i = 1,\cdots,7$), are identified by applying the algorithm in Section 5.4. Figure 9 shows identified values. Note that position-independent terms identified above are included as an offset.

(3)   Identification of position-dependent geometric errors of C-axis

Position-dependent geometric errors of C-axis, namely $\delta x_{CB}(B_i^*, C_j^*)$, $\delta y_{CB}(B_i^*, C_j^*)$, $\delta z_{CB}(B_i^*, C_j^*)$, $\alpha_{CB}(B_i^*, C_j^*)$, $\beta_{CB}(B_i^*, C_j^*)$, and $\gamma_{CB}(B_i^*, C_j^*)$ ($i = 1,\cdots,7$, $j = 1,\cdots,12$), are identified by applying the algorithm in Section 5.5. Identified values at $B_i^* = -90°$ and $0°$ are shown in Figs. 10 and 11, respec-

tively.

(4) *Observation*

In Figs. 9 to 11, no significant position-dependent error is observed both on B- and C-axes in this particular machine. The angular-dependent variation in tilt error motions of B- and C-axes is smaller than about 3×10^{-3} deg over $180°$ (for B-axis) or $330°$ (for C-axis). The B-axis angular positioning error at $B_i^* = -90°$ is only -1.5×10^{-3} deg.

7 Conclusion

- Compared to ball bar measurements [3,5,6,7,8], the R-test has a strong potential advantage in its applicability to high-efficient, *fully-automated* calibration of "error map" of five-axis machine tools in their mass-production.
- The "error map" of five-axis kinematics is parameterized by position-dependent geometric errors of each axis. The algorithm presented in Section 5 aims to separate the table's error motion, measured by the R-test in relative to the spindle, into the error map of each rotary axis.
- Its application example is presented in Section 6 to experimentally demonstrate the construction of error map of each rotary axis.
- The measurement uncertainty analysis of the R-test device itself was presented in [24,27]. The uncertainty in the present scheme will be studied in more details in our future research.

References

[1] ISO 10791-1, Test conditions for machining centres – Part 1: Geometric tests for machines with horizontal spindle and with accessory heads (horizontal Z-axis),

21

1998.

[2] ISO 230-7, Test code for machine tools – Part 7: Geometric accuracy of axes of rotation, 2006.

[3] Abbaszaheh-Mir, Y., Mayer, J. R. R., Clotier, G., Fortin, C., Theory and simulation for the identification of the link geometric errors for a five-axis machine tool using a telescoping magnetic ball-bar, International Journal of Production Research, 40, 18 (2002) 4781–4797.

[4] Zargarbashi, S.H.H. Mayer, J.R.R., Single setup estimation of a five axis machine tool eight link errors by programmed end point constraint and on the fly measurement with Capball sensors, International Journal of Machine Tools and Manufacture, 49 (2009) 759-766.

[5] Kakino, Y., Ihara, T., Sato, H., Otsubo, H., A Study on the motion accuracy of NC machine tools (7th report) –Measurement of motion accuracy of 5-axis machine by DBB tests–, Journal of Japan Society for Precision Engineering, 60, 5 (1994) 718–723 (in Japanese).

[6] Tsutsumi, M., Saito, A., Identification and compensation of systematic deviations particular to 5-axis machining centers, International Journal of Machine Tools and Manufacture, 43 (2003) 771–780.

[7] Tsutsumi, M., Saito, A., Identification of angular and positional deviations inherent to 5-axis machining centers with a tilting-rotary table by simultaneous four-axis control movement, International Journal of Machine Tools and Manufacture, 44 (2004) 1333–1342.

[8] Lei, W. T., Sung, M. P., Liu, W. L., Chuang, Y. C., Double ballbar test for the rotary axes of five-axis CNC machine tools, International Journal of Machine Tools and Manufacture, 47 (2007) 273–285.

[9] Tsutsumi, M., Ihara, Y., Saito, A., Mishima, N., Ibaraki, S., Yamamoto, M., Kobayashi, M., Yonetani, T., Standardization of testing methods for kinematic

22

motion of five-axis machining centers – Draft proposal for ISO standard –, In: Proc. of the 7th Manufacturing and Machine Tool Conference, 2008, 95-96 (in Japanese).

[10] ISO/CD 10791-6:2009, Test Conditions for Machining Centers – Part 6: Accuracy of Feeds, Speeds and Interpolations.

[11] Weikert, S., R-Test, a New Device for Accuracy Measurements on Five Axis Machine Tools, Annals of the CIRP, 53, 1 (2004) 429–432.

[12] Bringmann, B., Knapp, W., Model-based 'Chase-the-Ball' calibration of a 5-axis machining center, Annals of the CIRP, 55, 1 (2006) 531–534.

[13] IBS Precision Engineering, `http://www.ibspe.com`

[14] Florussen, G. H. U., Spaan H. A. M., Static R-Test: Allocating the Centreline of Rotary Axes of Machine Tools, In: Proc. of the 8th Lamdamap Conference, (2007) 196–202.

[15] Fidia S.p.a., `http://www.fidia.it/`

[16] Schwenke, H., Knapp, W., Haitjema, H., Weckenmann, A., Schmitt, R., Delbressine, F., Geometric error measurement and compensation of machines –An update, CIRP Annals - Manufacturing Technology, 57, 2 (2008) 560–575.

[17] Uddin, M. S., Ibaraki, S., Matsubara, A., Matsushita, T., Prediction and compensation of machining geometric errors of five-axis machining centers with kinematic errors, Precision Engineering, 33, 2 (2009) 194–201.

[18] Veldhuis, S. C., Elbestawi M. A., A strategy for the compensations of the errors in five-axis machining, Annals of the CIRP, 44, 1 (1995) 373–377.

[19] Mahbubur, R. M. D., Heikkala, J., Lappalainen, K., Karjalainen, J. A., Positioning accuracy improvement in five-axis milling by postprocessing, Int. J. Mach. Tool. Manuf., 37, 2 (1997) 223–236.

[20] Lee D., Zhu Z., Lee K., Yang S.. Identification and Measurement of Geometric Error of 5-axis Machine Tool with Tilting Head using Double Ball Bar, In: Proc. of the 3rd International Conference of Asian Society for Precision Engineering and Nanotechnology, (2009).

[21] Inasaki, I., Kishinami, K., Sakamoto, S., Sugimura, N., Takeuchi, Y., Tanaka, F., *Shaper generation theory of machine tools – its basis and applications*, Yokendo, Tokyo, 1997 (in Japanese).

[22] Hong, C., Ibaraki, S., Matsubara, A., Influence of Position-dependent Geometric Errors of Rotary Axes on a Machining Test of Cone Frustum by Five-axis Machine Tools, To appear in *Precision Engineering*, 2010.

[23] Ibaraki, S., Iritani, T., Matsushita, T., Error Calibration on Five-axis Machine Tools by on-the-machine Measurement of Artifacts using a Touch-trigger Probe, *Proc. of 4th CIRP International Conference on High Performance Cutting*, (2010).

[24] Bringmann, B., Knapp, W., Machine tool calibration: Geometric test uncertainty depends on machine tool performance, Precision Engineering, 33 (2009) 524-529.

[25] Soons, J. A., Theuws, F.C., Schllekens, P.H., Modeling the errors of multi-axis machines: a general methodology, Precision Engineering, 14, 1 (1992), 5–19.

[26] Srivastava, A. K., Veldhuis, S. C., Elbestawit, M. A., Modelling geometric and thermal errors in a five-axis CNC machine tool, International Journal of Machine Tools and Manufacture. 35, 9 (1995), 1321–1337.

[27] Bringmann, B., (2007) Improving Geometric Calibration Methods for Multi-axes Machining Centers by Examining Error Interdependencies Effects, 2/664. Fortschritt-Berichte VDI, Düsseldorf.

List of Tables

List of Figures

25

Table 1

Location errors for the machine configuration in Fig. 1.

Symbol [21]	Symbol [2]	Description [2]
Location errors associated with rotary axes		
α_{BY}^0	A0B	Squareness error of B- to Z-axis
β_{BY}^0	B0B	Orientation of B-axis around Y-axis
γ_{BY}^0	C0B-C0Y	Squareness error of B- to X-axis
α_{CB}^0	A0C-A0B	Squareness error of C- to B-axis
δx_{BY}^0	X0B	Linear offset of B-axis in X direction
δy_{BY}^0	Y0B	Linear offset of B-axis in Y direction
δz_{BY}^0	Z0B	Linear offset of B-axis in Z direction
δy_{CB}^0	Y0C-Y0B	Linear offset of C-axis from B-axis in Y
Location errors associated with linear axes		
γ_{YX}^0	C0Y	Squareness error of Y- to X-axis
α_{ZY}^0	A0Z	Squareness error of Z- to Y-axis
β_{ZX}^0	B0Z	Squareness error of Z- to X-axis

Table 2

Position-dependent geometric errors for the machine configuration shown in Fig. 1 (global coordinate system (X-Y-Z) and B-axis coordinate system (^{b}X-^{b}Y-^{b}Z).

Symbol	Symbol [2]	Description
Position-dependent geometric errors of rotary axes		
$\alpha_{BY}(B)$	EAB	Tilt error motion of B-axis around X-axis
$\beta_{BY}(B)$	EBB	Angular positioning error of B-axis
$\gamma_{BY}(B)$	ECB-C0Y	Tilt error motion of B-axis around Z-axis
$\alpha_{CB}(C,B)$	EAC-EAB	Tilt error motion of C-axis around ^{b}X-axis
$\beta_{CB}(C,B)$	EBC-EBB	Tilt error motion of C-axis around ^{b}Y-axis
$\gamma_{CB}(C,B)$	ECC-ECB	Angular positioning error of C-axis
$\delta x_{BY}(B)$	EXB	Radial error motion of B-axis in X-direction
$\delta y_{BY}(B)$	EYB	Axial error motion of B-axis
$\delta z_{BY}(B)$	EZB	Radial error motion of B-axis in Z-direction
$\delta x_{CB}(C,B)$	EXC-EXB	Radial error motion of C-axis in ^{b}X-direction
$\delta y_{CB}(C,B)$	EYC-EYB	Radial error motion of C-axis in ^{b}Y-direction
$\delta z_{CB}(C,B)$	EZC-EZB	Axial error motion of C-axis
Position-dependent geometric errors of linear axes		
$\gamma_{YX}(Y)$	ECY	Yaw of Y-axis
$\alpha_{YX}(Y)$	EAY	Pitch of Y-axis
$\beta_{YX}(Y)$	EBY	Roll of Y-axis
$\delta x_{YX}(Y)$	EXY	Straightness error of Y-axis in X
$\delta y_{YX}(Y)$	EYY	Linear positioning error of Y-axis
$\delta z_{YX}(Y)$	EZY	Straightness error of Y-axis in Z
. . .		. . .

Table 3

Major specifications of the linear displacement probe.

Measuring principle	Photo-electric scanning of an incremental scale with spring-tensioned plunger
Measurement range	12 mm
System accuracy	$\pm 0.2 \mu$m
Gauging force (vertically upward)	0.35 to 0.6 N
Signal period	2 μm
Mechanically permissible traversing speed	30 m/min

Table 4

Major specifications of the experimental machining center.

axis	X	Y	Z	B	C
Stroke	850mm	450mm	450mm	$\pm 110°$	$360°$
Drive	servo motor + ball screw			direct drive	servo motor + worm gear
Max. speed				20 min^{-1}	100 min^{-1}
Guide way	slide guide way			tapered-roller bearing	ball bearing
Table size	ϕ400mm				

Table 5

Identified position-independent error terms.

Symbol	Identified value
α_{BY}^0	-1.0×10^{-3} deg
β_{BY}^0	0.2×10^{-3} deg
γ_{BY}^0	-0.5×10^{-3} deg
α_{CB}^0	1.3×10^{-3} deg
δx_{BY}^0	6.4×10^{-3} mm
δy_{BY}^0	7.8×10^{-3} mm
δz_{BY}^0	-13.2×10^{-3} mm
δy_{CA}^0	-3.4×10^{-3} mm
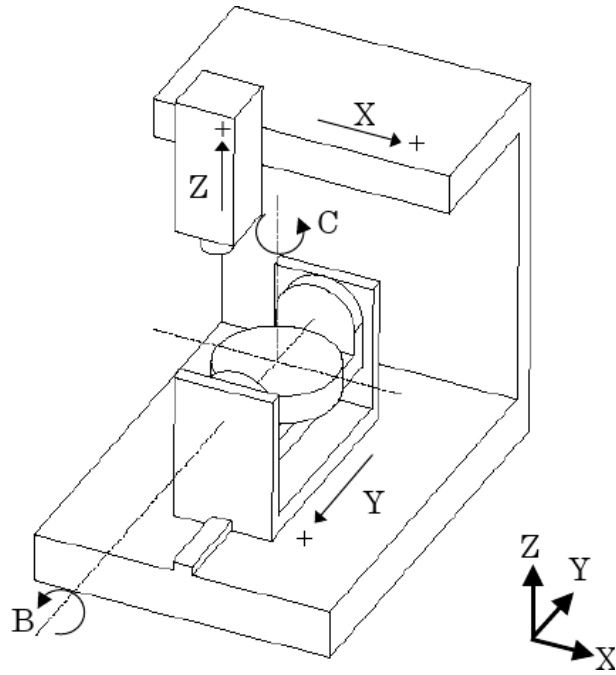
Fig. 1. The configuration of a five-axis machine tool considered in this paper.
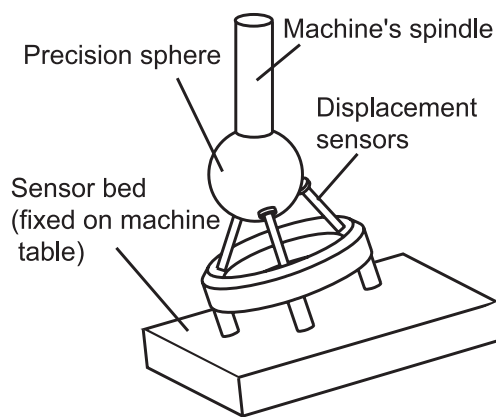
Fig. 2. R-test device.
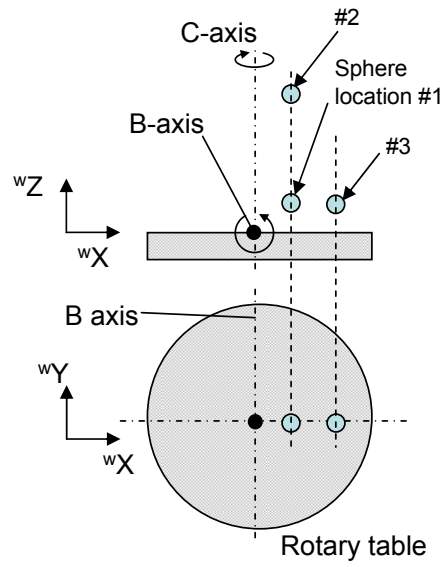
Fig. 3. Reference sphere locations to identify the orientation of C-axis.
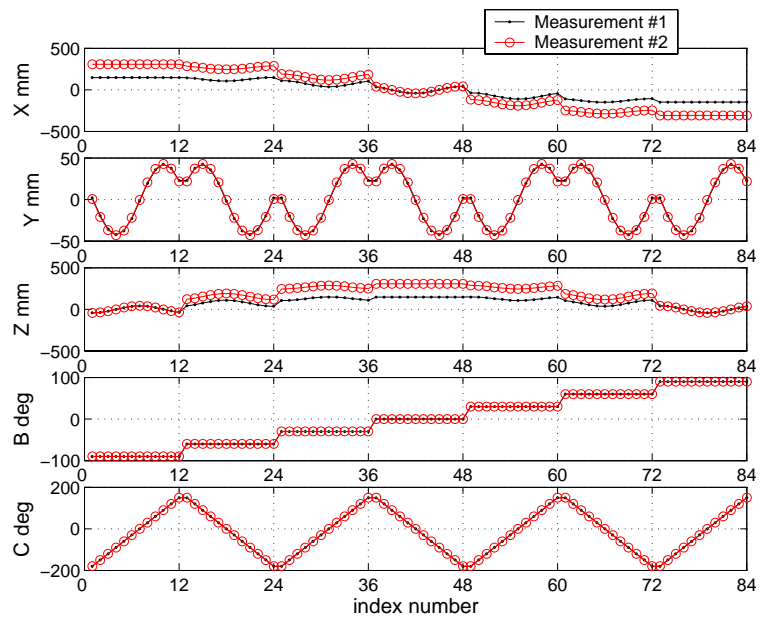
Fig. 4. Command X^*, Y^*, Z^*, B^*, and C^* trajectories.

33
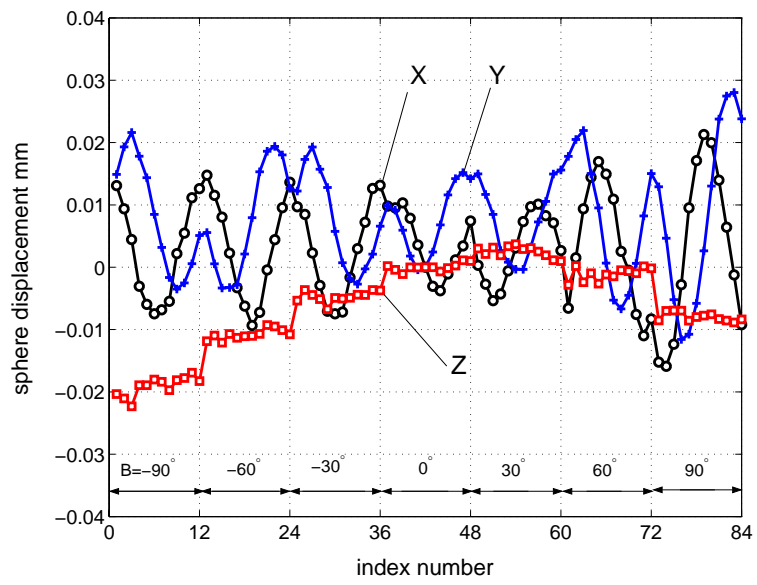
Fig. 5. Measured sphere displacements in the workpiece coordinate system, $^w\bar{q}(B_i^*, C_j^*)$, (Measurement #1).
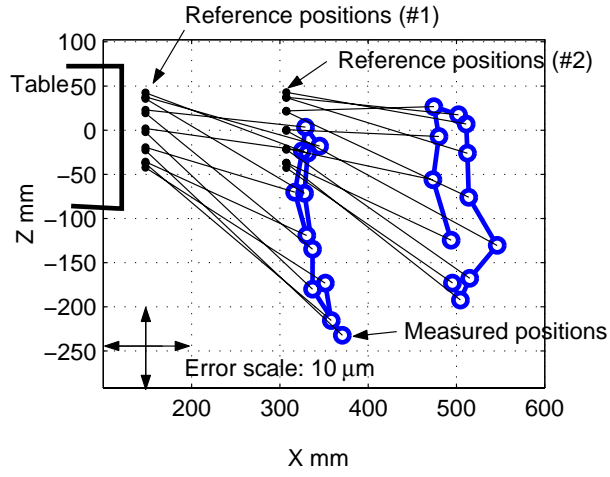
(a) $B_i^* = -90°$.
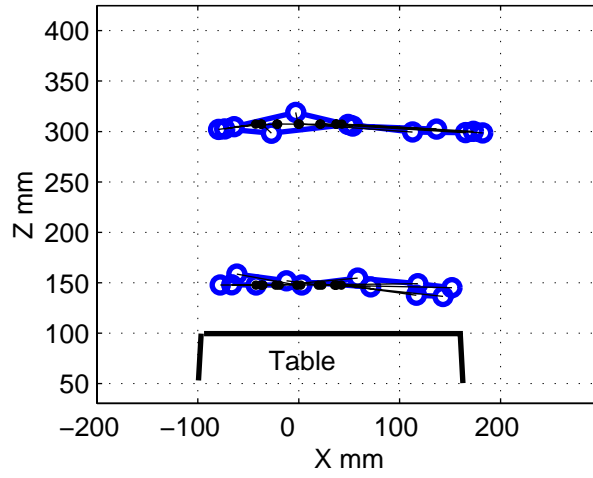
(b) $B_i^* = 0°$.

Fig. 6. Measured sensor displacements in the global coordinate system, $-{}^r\bar{q}_k(B_i^*, C_j^*)$(Measurements #1 and #2).
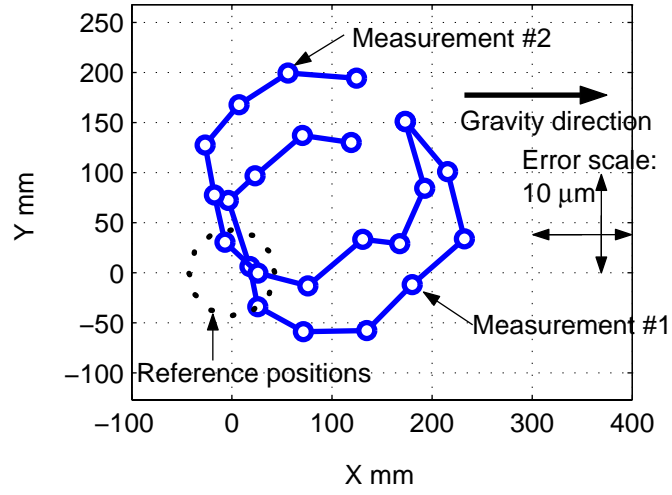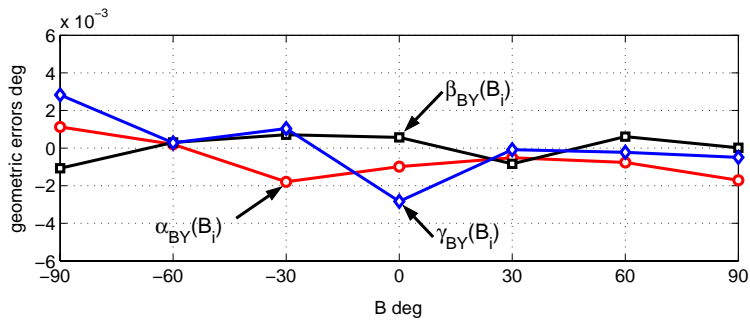
(a) $B_i^* = -90°$.
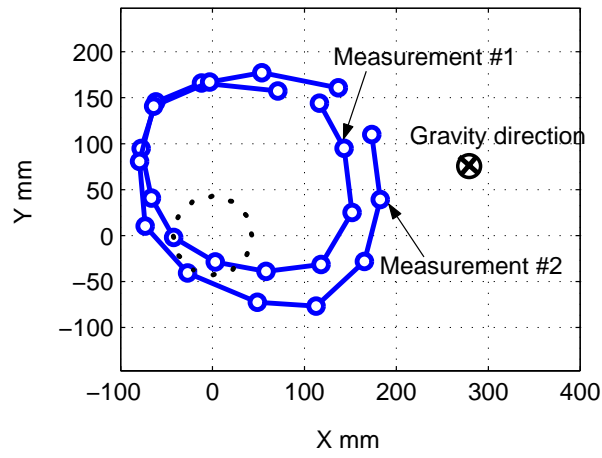
(b) $B_i^* = 0°$.

Fig. 7. Measured sensor displacements in the B-axis coordinate system, $-{}^b\bar{q}_k(B_i^*, C_j^*)$ (Measurements #1 and #2).
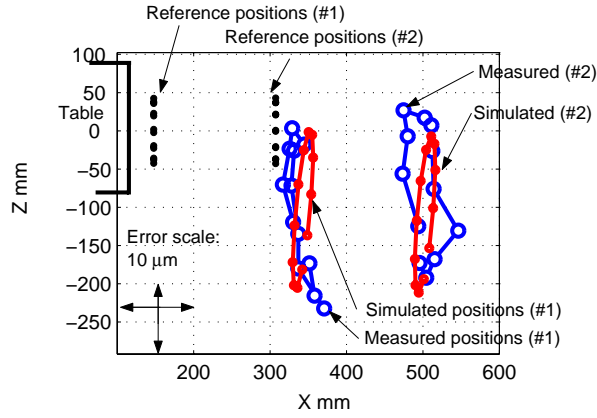
Fig. 8. Comparison of measured sensor displacements and the simulated influence of identified position-independent terms shown in Table 5 in the global coordinate system (at $B_i^* = -90°$, projected onto the XZ plane).
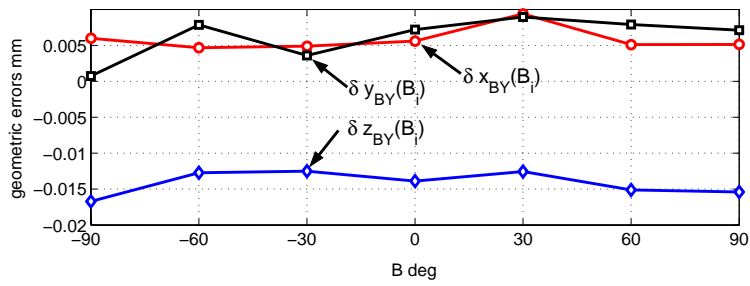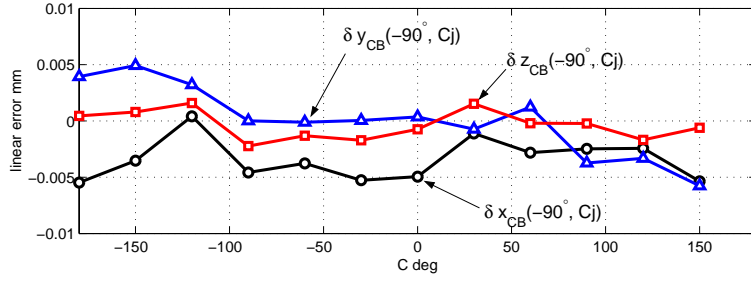

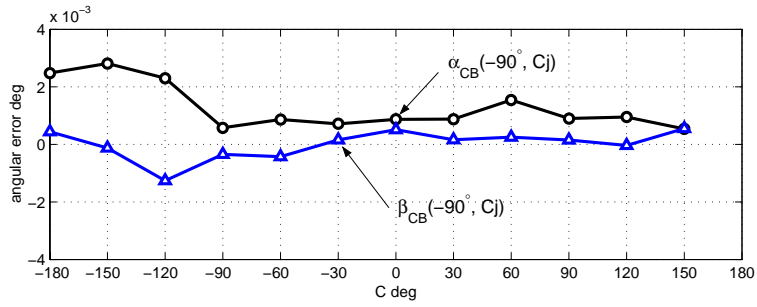(a) $\delta x_{BY}(B_i^*)$, $\delta y_{BY}(B_i^*)$, and $\delta z_{BY}(B_i^*)$.

(b) $\alpha_{BY}(B_i^*)$, $\beta_{BY}(B_i^*)$, and $\gamma_{BY}(B_i^*)$.

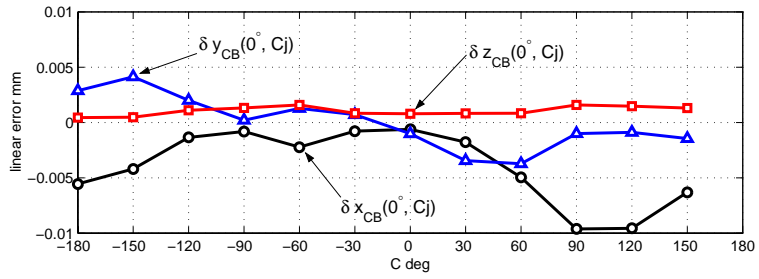Fig. 9. Identified position-dependent geometric errors of B-axis.

(a) $\quad \delta x_{CB}\big({-}90^\circ, C_j^*\big), \qquad \delta y_{CB}\big({-}90^\circ, C_j^*\big), \qquad$ and $\delta z_{CB}\big({-}90^\circ, C_j^*\big)$.

(b) $\quad \alpha_{CB}\big({-}90^\circ, C_j^*\big), \qquad \beta_{CB}\big({-}90^\circ, C_j^*\big), \qquad$ and $\gamma_{CB}\big({-}90^\circ, C_j^*\big)$.

Fig. 10. Identified position-dependent geometric errors of C-axis at $B_i = -90^\circ$.

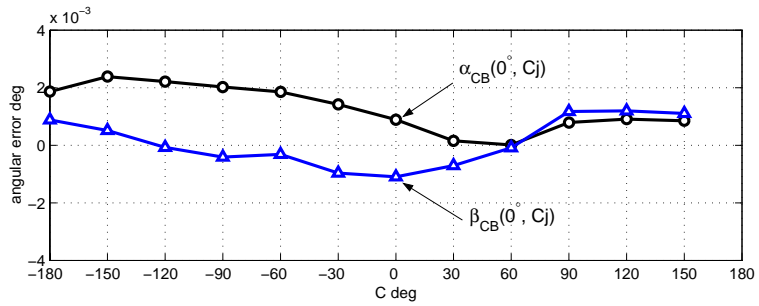(a) $\delta x_{CB}(0^\circ, C_j^*)$, $\delta y_{CB}(0^\circ, C_j^*)$, and $\delta z_{CB}(0^\circ, C_j^*)$.

(b) $\alpha_{CB}(0^\circ, C_j^*)$, $\beta_{CB}(0^\circ, C_j^*)$, and $\gamma_{CB}(0^\circ, C_j^*)$.

Fig. 11. Identified position-dependent geometric errors of C-axis at $B_i = 0^\circ$.